Acta Cryst E CRYSTALLOGRAPHIC COMMUNICATIONS

ISSN 2056-9890

Crystal structure and Hirshfeld surface analysis of 1,5-naphthyridine-1,5-diium dichloride

Valerii Y. Sirenko,[a]* Alexandru-Constantin Stoica,[b] Olena V. Prysiazhna,[c,d] Vadim A. Potaskalov[e] and Irina A. Golenya[a]

[a]Department of Chemistry, Taras Shevchenko National University of Kyiv, Volodymyrska St. 64/13, 01601 Kyiv, Ukraine, [b]'Petru Poni' Institute of Macromolecular Chemistry, Aleea Gr. Ghica Voda 41A, 700487 Iasi, Romania, [c]Bakul Institute for Superhard Materials, National Academy of Sciences of Ukraine, Avtozavods'ka St. 2, Kyiv 04074, Ukraine, [d]Institute of Innovative Education, Kyiv National University of Construction and Architecture, Osvity St. 4, Kyiv 03037, Ukraine, and [e]Department of General and Inorganic Chemistry, National Technical University of Ukraine Igor Sikorsky Kyiv Polytechnic Institute, Beresteiskyi Pr. 37, 03056 Kyiv, Ukraine. *Correspondence e-mail: valerii_sirenko@knu.ua

Received 27 October 2026
Accepted 19 November 2026

Edited by K. V. Domasevitch, National Taras Shevchenko University of Kyiv, Ukraine

Keywords: crystal structure; organic cation; hydrogen bonding; anion–π interactions; Hirshfeld surface analysis.

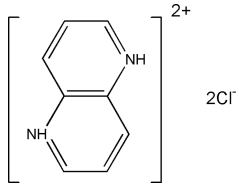
CCDC reference: 2604849

Supporting information: this article has supporting information at journals.iucr.org/e

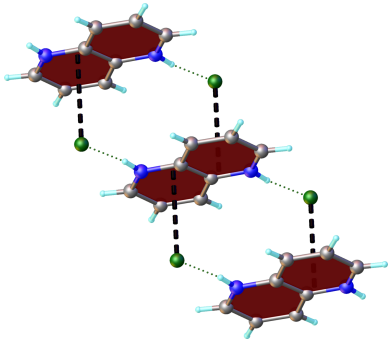
The crystal structure of the title compound, $C_8H_8N_2^{2+}\cdot 2Cl^-$, containing a centrosymmetric dication of diprotonated 1,5-naphthyridine, is reported. The compound crystallizes in the triclinic space group $P\overline{1}$, with the dication situated across an inversion centre. Protonation does not substantially alter the geometry of the fused heteroaromatic framework compared with neutral 1,5-naphthyridine. The crystal packing is governed primarily by N—H···Cl hydrogen bonds, C—H···Cl contacts and anion–π interactions, resulting in a layered supramolecular arrangement. Hirshfeld surface analysis and two-dimensional fingerprint plots reveal that H···Cl contacts make the largest contribution to the intermolecular contact surface (30.8%), while C···Cl and N···Cl contacts, associated with anion–π interactions, account for 6.9 and 1.6% of the total, respectively. The results provide insight into the intermolecular interactions governing the crystal packing of protonated 1,5-naphthyridine.

1. Chemical context

Nitrogen-containing heterocycles are important building blocks in crystal chemistry owing to their diverse electronic properties and ability to participate in a range of intermolecular interactions. The presence of N atoms within aromatic rings influences electron distribution, basicity and hydrogen-bonding capabilities, providing multiple possibilities for directing molecular organization in the solid state (Desiraju, 2007; Subramanian & Zaworotko, 1994). Fused aza-aromatic systems are particularly interesting in this respect, as their rigid conjugated frameworks can participate in hydrogen bonding, aromatic stacking and electrostatic interactions, contributing to the formation of diverse supramolecular architectures (Desiraju, 2007). Interactions between organic cations and halide anions play a key role in the supramolecular organization and structural stability of hybrid perovskite-like systems (El–Mellouhi *et al.*, 2016).



Protonation provides an effective means of modifying the intermolecular interaction patterns of nitrogen-containing heterocycles. Protonation of a nitrogen containing hetero-



OPEN ACCESS
Published under a CC BY 4.0 licence

cyclic ring changes the charge distribution of the system and introduces additional hydrogen-bond donor functionality. In the resulting salts, charge-assisted hydrogen bonds between protonated heterocycles and counter-anions frequently play a central role in crystal packing (Stevens *et al.*, 2014).

Among the less conventional intermolecular interactions relevant to crystal chemistry are anion–π interactions, which involve contacts between anions and the π-systems of aromatic rings. Although initially considered unfavourable because of the negative charge of the anion, such interactions have been established experimentally and theoretically, particularly for electron-deficient aromatic systems (Gural'skiy *et al.*, 2006; Gural'skiy *et al.*, 2009; Schottel *et al.*, 2008). Their strength and geometry depend on the electronic properties of the aromatic ring, the nature of the anion and the surrounding molecular environment. Anion–π interactions may also cooperate with hydrogen bonding, contributing to molecular recognition and the organization of supramolecular assemblies (Plais *et al.*, 2023; Giese *et al.*, 2016; Bauzá *et al.*, 2016). In protonated heterocycles, the positively charged aromatic framework may additionally influence anion positioning through electrostatic attraction; however, the assignment of a specific anion–π interaction requires consideration of the contact geometry and the electronic characteristics of the interacting species (Plais *et al.*, 2023).

1,5-Naphthyridine is a fused diaza-aromatic compound containing two pyridine-like N atoms, making it a suitable building block for investigating the structural consequences of protonation (Fuertes *et al.*, 2020). In medicinal chemistry, 1,5-naphthyridine compounds exhibit a broad spectrum of biological activities, including antiproliferative (Perez *et al.*, 2017), antibacterial (Magee *et al.*, 2009), antiparasitic (Zhu *et al.*, 2007) and antiviral effects (Selaković *et al.*, 2019), often acting as enzyme inhibitors (Nishimura *et al.*, 2011) or anti-inflammatory agents (Mirguet *et al.*, 2014). Beyond their pharmacological relevance, chelate complexes of 4-hydroxy-1,5-naphthyridines with group III metal ions (Al^{3+}, Ga^{3+} or In^{3+}) have been investigated as genuine deep-blue-emitting counterparts to the well-known green emitter tris(8-hydroxyquinoline)aluminium for organic light-emitting diodes (Lee *et al.*, 2011; Liao *et al.*, 2009; Poloek *et al.*, 2014; Poloek *et al.*, 2015). Furthermore, 1,5-naphthyridine-based ligands have been employed to construct single-molecule magnets (SMMs) (Bi *et al.*, 2016), which represent appealing multifunctional candidates for molecular spintronics and quantum computing applications. When coordinated to europium ions, naphthyridine ligands also form photoluminescent complexes characterized by high quantum yields, as well as enhanced thermal and photostability (Wei *et al.*, 2016). In addition, 1,5-naphthyridine derivatives show strong potential as thermally activated delayed fluorescence (TADF) emitters for OLED devices (Zhou *et al.*, 2019), while their aluminium chelates have been explored as exciton-blocking layers that extend the operational lifetime of organic photovoltaic cells (Liu *et al.*, 2010; Lee *et al.*, 2012). In the field of energy storage, 1,5-naphthyridine compounds have been evaluated with respect to their energy density and open-circuit potential (Araujo *et al.*, 2012), and selected derivatives have shown promise as anode film-forming additives and non-aqueous electrolyte components for lithium-ion batteries (Park *et al.*, 2014). Moreover, a *trans*-diaquadioxalatochromate(III) dihydrate salt containing a 1,5-naphthyridine has been described as a semiconductor material (Dridi *et al.*, 2018).

As part of our studies in this area, we now describe the synthesis and structure of the title compound, 1,5-naphthiridine hydrochloride.

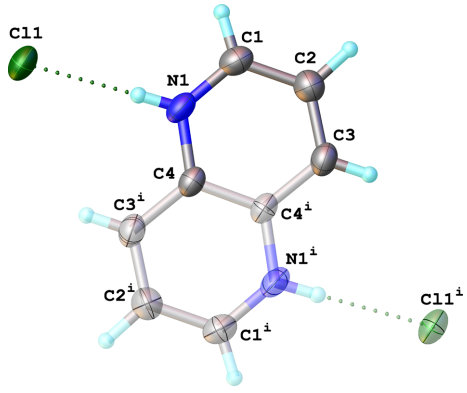


Figure 1
The molecular structure of the title compound, showing the atom-labelling scheme. Displacement ellipsoids are shown with 50% probability. [Symmetry code: (i) $-x+1, -y+1, -z+1$.]

2. Structural commentary

The title compound crystallizes in the triclinic space group $P\overline{1}$ with one formula unit per unit cell. The dication is situated across a crystallographic inversion centre at the mid-point of the C4—C4^{i} bond (Fig. 1). The C—N and C—C bond lengths in the dication are comparable to those in neutral 1,5-naphthyridine (van den Ham *et al.*, 1978), with differences between corresponding bonds not exceeding approximately 0.012 Å. The C1—N1 and C4—N1 bond lengths are 1.325 (4) and 1.361 (4) Å, respectively, within the range observed in the neutral molecule (1.315–1.368 Å). The C1—C2, C2—C3, C3—C4^{i} and C4—C4^{i} bond lengths are 1.396 (5), 1.358 (5), 1.415 (4) and 1.391 (6) Å, respectively. Thus, the pattern of shorter and longer bonds within the fused-ring system is retained upon protonation. Bond angles in the heterocyclic ring range from 118.2 (3) to 122.5 (3)°. In contrast to the small changes in bond lengths, the C—N—C angle increases from approximately 116.1–116.5° in the neutral molecule to 122.5 (3)° in the dication. A similar trend is observed in the monoprotonated 1,5-naphthyridinium cation, which features both protonated and unprotonated nitrogen sites: the C—N(H)—C angle at the protonated N atom is 121.1 (4)°, whereas the C—N—C angle at the unprotonated N atom remains significantly smaller at 117.3 (4)° (Kobayashi *et al.*, 2014). Such a pronounced difference between the C—N—C and C—N(H)—C angles provides a reliable geometric criterion for unambiguously assigning the protonation site in 1,5-naphthyridine derivatives. Furthermore, in a diprotonated 1,5-naphthyridine derivative bearing electron-donating

Table 1
Hydrogen-bond geometry (Å, °).

D—H···A	D—H	H···A	D···A	D—H···A
N1—H1N···Cl1	0.80 (5)	2.17 (5)	2.969 (2)	171 (4)
C1—H1···Cl1^{i}	0.91 (4)	2.67 (4)	3.584 (3)	174 (3)
C2—H2···Cl1^{ii}	1.01 (4)	2.83 (4)	3.532 (3)	127 (3)

Symmetry codes: (i) $-x, -y+1, -z$; (ii) $x+1, y+1, z$.

substituents (Wiesner *et al.*, 2023), the C—N(H)—C angle is 121.6 (3)°, which is in close agreement with the value observed for the unsubstituted 1,5-naphthyridinium dication reported in this work. This behaviour can be rationalized by protonation involving the in-plane nitrogen lone pairs, which do not participate in the aromatic π-system, thereby preserving π-conjugation while modifying the local geometry at nitrogen.

3. Supramolecular features

The positive charge of diprotonated 1,5-naphthyridine is balanced by chloride counter-ions. The N—H···Cl hydrogen bonds provide the principal directional interactions between the dications and chloride anions, while the weaker C—H···Cl contacts further contribute to the supramolecular arrangement (Table 1). These hydrogen bonds link the dications and chloride anions into supramolecular layers parallel to the ($\bar{1}$11) plane (Fig. 2).

The interlayer separation between adjacent supramolecular planes is 3.13 Å, which is noticeably shorter than the sums of the van der Waals radii for C and Cl (3.45 Å) and for N and Cl (3.30 Å) [r(vdW): C = 1.70 Å, N = 1.55 Å and Cl = 1.75 Å]. This compact interlayer spacing is accommodated by a slight displacement (0.22 Å) of the Cl^{-} anion out of the mean plane

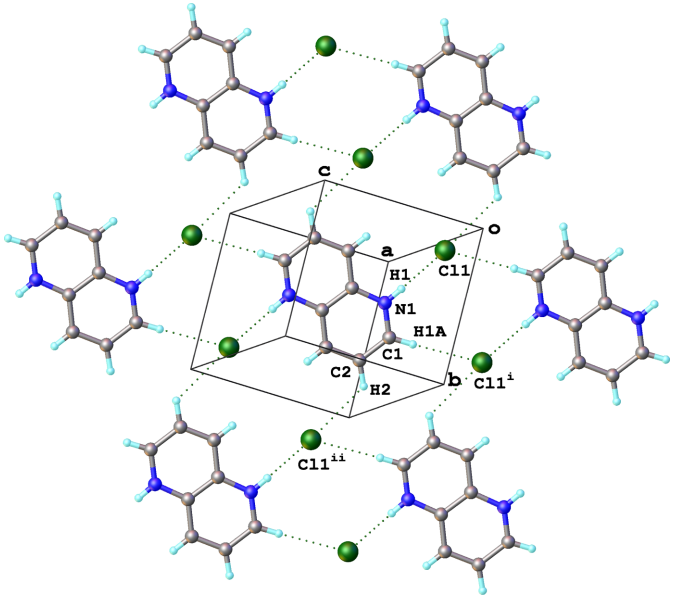


Figure 2
Fragment of the crystal structure showing propagation of supramolecular two-dimensional layers parallel to the ($\bar{1}$11) plane. [Symmetry codes: (i) $-x, -y+1, -z$; (ii) $x+1, y+1, z$.]

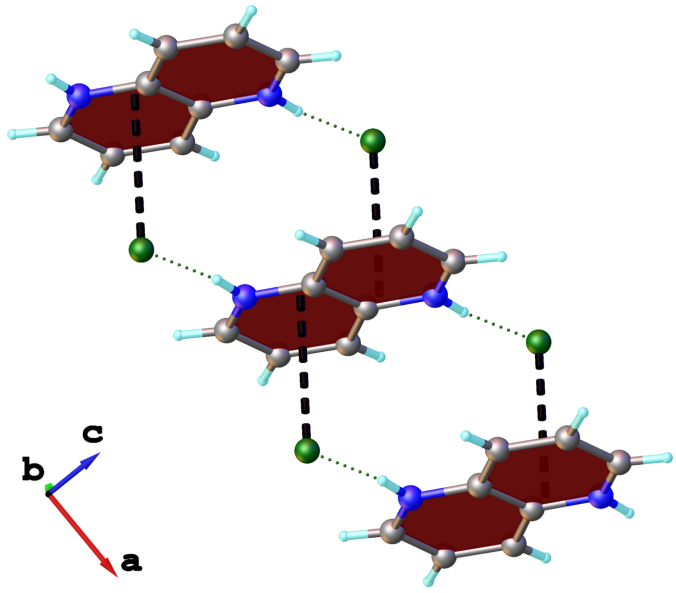


Figure 3
Fragment of the crystal structure showing the supramolecular assembly of the 1,5-naphthyridinium cations and chloride anions mediated through N—H···Cl hydrogen bonds (green dotted lines) and anion–π interactions (black dashed lines showing the orthogonal projections of the Cl^{-} anions onto the shaded ring planes).

of the naphthyridine rings and a lateral offset of adjacent layers relative to one another, consistent with attractive interlayer anion–cation interactions (Fig. 3).

Closer inspection of these anion–π interactions between the Cl^{-} anions and the 1,5-naphthyridinium dication reveals a significant electrostatic contribution, manifested in the off-centre shift of the chloride ion away from the ring centroid toward the positively charged bridgehead C4 atom [Fig. 4(*a*)]. This displacement results in a perpendicular distance of 3.330 (1) Å from the Cl^{-} anion to the ring plane and a short interatomic C4···Cl1 distance of 3.368 (3) Å – which remains shorter than the sum of the van der Waals radii (3.45 Å) – compared to the Cl···centroid distance of 3.448 (1) Å. Each dication forms identical off-centre anion–π contacts with two inversion-related chloride anions positioned on opposite sides of its molecular plane (Fig. 4).

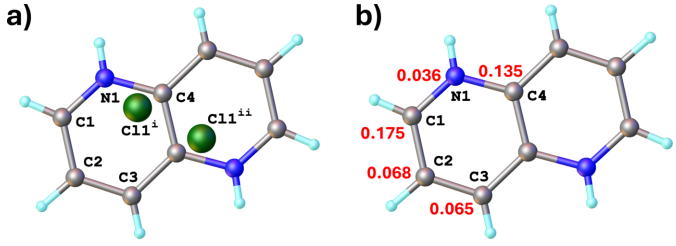


Figure 4
(*a*) Orthogonal projections of the Cl1^{i} and Cl1^{ii} anions onto the mean plane of the 1,5-naphthyridinium ring. (*b*) DFT-calculated Hirshfeld charges of the 1,5-naphthyridine-1,5-diium dication. [Symmetry codes: (i) $x+1, y, z$; (ii) $-x, -y+1, -z+1$.]

Table 2
Calculated Hirshfeld atomic charges for the 1,5-naphthyridine-1,5-diium dication and neutral 1,5-naphthyridine.

Atom	Hirshfeld charge (*e*)
1,5-Naphthyridine-1,5-diium (this work)	
N1	0.036
H1N	0.183
C1	0.175
H1	0.121
C2	0.068
H2	0.120
C3	0.065
H3	0.098
C4	0.135
1,5-Naphthyridine (DAZNAR; van den Ham *et al.*, 1978)	
N1	−0.166
N2	−0.161
C1	0.030
H1	0.052
C2	−0.052
H2	0.050
C3	−0.017
H3	0.057
C4	0.024
H4	0.049
C5	−0.048
H5	0.054
C6	−0.021
H6	0.057
C7	0.044
C8	0.046

Further analysis of the calculated Hirshfeld atomic charges for the 1,5-naphthyridine-1,5-diium dication and neutral non-protonated 1,5-naphthyridine (CSD refcode DAZNAR; van den Ham *et al.*, 1978) confirms a pronounced redistribution of electron density upon diprotonation [Table 2 and Fig. 4(*b*)]. Whereas in neutral 1,5-naphthyridine the N atoms carry negative charges, protonation reverses the partial charge on N1 and strongly polarizes the adjacent ring C atoms. Specifically, the positive charge within the heterocyclic ring is predominantly localized on the α-carbon atom C1 and the bridgehead carbon C4, with the Hirshfeld charge on C4 increasing threefold compared to that in the neutral molecule. Since the peripheral C1—H1 and N1—H1N groups are engaged in in-plane hydrogen bonding, the positively charged and sterically accessible bridgehead C atom serves as the primary electrophilic site for out-of-plane interactions, which directly accounts for the observed off-centre displacement of the Cl^- anions toward C4.

It is instructive to compare this arrangement with related salts of protonated electron-deficient bicyclic nitrogen heterocycles. For instance, anion–π contacts have been documented in protonated 1,5-naphthyridinium chloranilate systems (Kobayashi *et al.*, 2014), where the O atom of the chloranilate anion interacts with the π-system of the cation. However, unlike the title structure – in which the halide anion shifts toward the positively polarized carbon backbone – the anionic O atom in the chloranilate salt is situated nearly directly above the ring centroid. By contrast, an off-centre geometry closely resembling that of our compound is

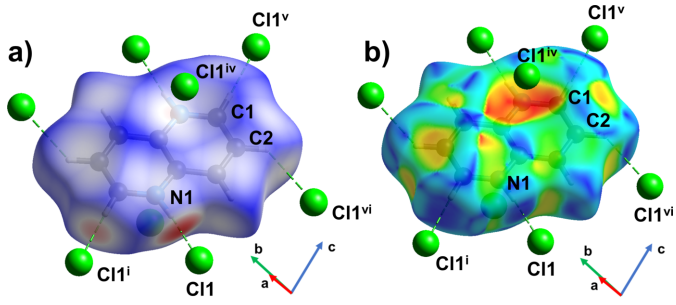


Figure 5
(*a*) Representation of the Hirshfeld surface of the 1,5-naphthyridine-1,5-diium cation, with the d_{norm} function plotted onto the surface to highlight various interactions. (*b*) The Hirshfeld surface mapped with the shape-index function highlights anion–π interactions. [Symmetry codes: (i) $-x$, $-y+1$, $-z$; (ii) $x+1$, $y+1$, z; (iii) $-x+1$, $-y+1$, $-z+1$; (iv) $-x$, $-y+1$, $-z+1$; (v) $x+1$, y, $z+1$; (vi) $-x$, $-y$, $-z+1$.]

observed in phthalazinium hydrochloride, where the Cl^- anion likewise resides above a positively polarized C atom rather than over the ring centroid (Bolte *et al.*, 2024). Conversely, in the related *N*,*N*′-diethylquinoxalinium diiodide system, the iodide anion adopts a more central position above the ring centroid (Hausen *et al.*, 1993). These examples highlight that different compositional and strutural features can affect the nature of anion–cation contacts in the case of aromatic heterocyclic cations.

4. Hirshfeld surface analysis

Hirshfeld surface analysis was performed using *CrystalExplorer21.5* (Spackman *et al.*, 2021) to characterize the intermolecular contacts in the crystal structure. The surfaces were mapped over d_{norm} using the standard resolution (−0.633 to 0.338 a.u.). A consistent colour scale was applied, with white areas representing contacts approximately equal to the sums of the van der Waals radii, while red and blue areas indicate contacts shorter and longer than these values, respectively [Fig. 5(*a*)]. The most pronounced red regions correspond to the N1—H1N···Cl1 contact (−0.626 a.u.) and C1—H1···$Cl1^i$ (−0.237 a.u.) and light-pink regions are observed for C2—H2···$Cl1^{ii}$ (−0.025 a.u.) and C···Cl interactions (−0.046 a.u.). Concave red regions (−0.874 a.u.) on the Hirshfeld surface mapped with the shape-index function [Fig. 5(*b*)] further indicate the presence of anion–π interactions in the compound.

The corresponding two-dimensional fingerprint plots were used to quantify the different types of intermolecular contacts and assess their relative contributions to the overall crystal packing. Cl···H contacts make the largest contribution (30.8%), while C···Cl and N···Cl contacts, associated with anion–π interactions, account for only 6.9 and 1.6% of the total, respectively (Fig. 6). All other contacts revealed on the Hirshfeld surface are not associated with well-defined directional intermolecular interactions and arise primarily from H atoms located at the ends of molecular fragments.

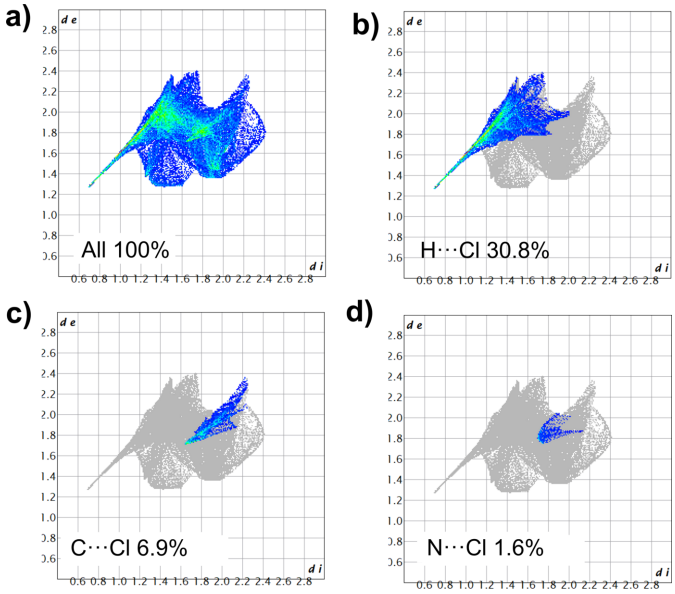


Figure 6
Two-dimensional fingerprint plots from a Hirshfeld surface analysis of the individual organic dications in the structure of 1,5-naphthyridine dihydrochloride showing (*a*) all contacts, (*b*) H···Cl (30.8%), (*c*) C···Cl (6.9%) and (*d*) N···Cl (1.6%).

5. Database survey

A search through the Cambridge Structural Database (CSD, Version 6.01, last update September 2026; Groom *et al.*, 2016) revealed 22 crystal structures containing a non-protonated 1,5-naphthyridine molecule (mostly as a ligand in different coordination compounds), including the crystal structure of 1,5-naphthyridine (DAZNAR; van den Ham *et al.*, 1978), the geometric parameters of which were used for comparison with the title compound in the *Structural commentary* section. Six more search hits contained monoprotonated 1,5-naphthyridine (*e.g.* XESNUH, MOGCAO, MOGCAO01, *etc.*; Cvrtila & Stilinović, 2017; Kobayashi *et al.*, 2014). Notably, the crystal structure of diprotonated 1,5-naphthyridine has not been reported before.

6. Charge distribution analysis

To evaluate the electronic redistribution upon protonation, non-periodic single-point density functional theory (DFT) calculations were performed on the isolated $C_8H_8N_2^{2+}$ dication (total charge +2) and neutral 1,5-naphthyridine molecule (total charge 0; CSD refcode DAZNAR: van den Ham *et al.*, 1978) directly at their experimental X-ray geometries without further geometry optimization. The calculations were carried out within the *Amsterdam Modeling Suite* (*AMS*, using the *BAND* engine; te Velde & Baerends, 1991; Philipsen *et al.*, 2025; Baerends *et al.*, 2025) employing the spin-restricted hybrid B3LYP exchange–correlation functional (Becke, 1993; Lee *et al.*, 1988; Stephens *et al.*, 1994). Scalar relativistic effects were taken into account *via* the zero-order regular approximation (ZORA; van Lenthe *et al.*, 1993, 1994). An all-electron triple-zeta polarized (TZP) basis set was used for all atoms with no frozen-core approximation, and the numerical integration quality was set to 'Good', which controls the precision of the numerical integration grid (Becke-type grid used in the AMS framework) and the quality of the ZLMfit density-fitting scheme employed to efficiently compute the Coulomb and exchange–correlation potentials for the molecular system. Partial atomic charges were derived using the Hirshfeld (Hirshfeld, 1977) population analysis scheme (Table 2).

Table 3
Experimental details.

Crystal data	
Chemical formula	$C_8H_8N_2^{2+}\cdot 2Cl^-$
M_r	203.06
Crystal system, space group	Triclinic, $P\overline{1}$
Temperature (K)	293
a, b, c (Å)	4.9408 (6), 6.3593 (6), 7.2897 (8)
α, β, γ (°)	81.946 (8), 80.375 (10), 80.067 (9)
V (Å^3)	220.97 (4)
Z	1
Radiation type	Mo $K\alpha$
μ (mm^{-1})	0.68
Crystal size (mm)	0.19 × 0.05 × 0.04
Data collection	
Diffractometer	Rigaku XtaLAB Synergy Dualflex diffractometer with a HyPix detector
Absorption correction	Analytical (*CrysAlis PRO*; Rigaku OD, 2024)
T_{min}, T_{max}	0.911, 0.982
No. of measured, independent and observed [$I > 2\sigma(I)$] reflections	2918, 1097, 917
R_{int}	0.032
(sin $\theta/\lambda)_{max}$ (Å^{-1})	0.708
Refinement	
$R[F^2 > 2\sigma(F^2)]$, $wR(F^2)$, S	0.065, 0.195, 1.05
No. of reflections	1097
No. of parameters	67
H-atom treatment	Only H-atom coordinates refined
$\Delta\rho_{max}$, $\Delta\rho_{min}$ (e Å^{-3})	0.94, −0.40

Computer programs: *CrysAlis PRO* (Rigaku OD, 2024), *SHELXT2018* (Sheldrick, 2015*a*), *SHELXL2019* (Sheldrick, 2015*b*) and *OLEX2* (Dolomanov *et al.*, 2009).

7. Synthesis and crystallization

10 mg of 1,5-naphthyridine was dissolved in 100 µl of concentrated aqueous HCl solution (37%) under heating and left to cool to room temperature. Within 1 h, colourless crystals suitable for X-ray analysis formed. The obtained crystals were stored in the mother liquor prior to measurement.

8. Refinement

Crystal data, data collection and structure refinement details are summarized in Table 3. All H atoms were localized from a Fourier difference map. Their coordinates were refined with U_{iso}(H) values set at 1.2U_{eq}(C) or 1.5U_{eq}(N) of the carrier C or N atoms. The moderate accuracy of the crystal structure determination is attributed to the quality of the lamellar crystals.

Acknowledgements

The authors are grateful to the FAIRE programme provided by the Cambridge Crystallographic Data Centre (CCDC) for the opportunity to use the Cambridge Structural Database (CSD) and associated software. The authors gratefully acknowledge SCM/AMS for their support and for providing access to the Amsterdam Modeling Suite, which enabled the density functional theory calculations presented in this study.

Funding information

Funding for this research was provided by: Ministry of Education and Science of Ukraine (grant No. 26BF037-01M).

References

Araujo, C. M., Simone, D. L., Konezny, S. J., Shim, A., Crabtree, R. H., Soloveichik, G. L. & Batista, V. S. (2012). *Energy Environ. Sci.* **5**, 9534–9542.

Baerends, E. J., Aguirre, N. F., Austin, N. D., Autschbach, J., Bickelhaupt, F. M., Bulo, R., Cappelli, C., van Duin, A. C. T., Egidi, F., Fonseca Guerra, C., Förster, A., Franchini, M., Goumans, T. P. M., Heine, T., Hellström, M., Jacob, C. R., Jensen, L., Krykunov, M. V., van Lenthe, E., Michalak, A., Mitoraj, M., Neugebauer, J., Nicu, V. P., Philipsen, P. H. T., Ramanantoanina, H., Rüger, R., Schreckenbach, G., Stener, M., Swart, M., Thijssen, J. M., Trnka, T., Visscher, L., Yakovlev, A. L. & van Gisbergen, S. J. A. (2025). *J. Chem. Phys.* **162**, 162501-1–162501-47.

Bauzá, A., Mooibroek, T. J. & Frontera, A. (2016). *CrystEngComm* **18**, 10–23.

Becke, A. D. (1993). *J. Chem. Phys.* **98**, 5648–5652.

Bi, Y., Chen, C., Zhao, Y.-F., Zhang, Y.-Q., Jiang, S.-D., Wang, B.-W., Han, J.-B., Sun, J.-L., Bian, Z.-Q., Wang, Z.-M. & Gao, S. (2016). *Chem. Sci.* **7**, 5020–5031.

Bolte, M., Kaehler, T. & Wagner, M. (2024). CSD Communication (CCDC 2331847). CCDC, Cambridge, England.

Cvrtila, I. & Stilinović, V. (2017). *Cryst. Growth Des.* **17**, 6793–6800.

Desiraju, G. R. (2007). *Angew. Chem. Int. Ed.* **46**, 8342–8356.

Dolomanov, O. V., Bourhis, L. J., Gildea, R. J., Howard, J. A. K. & Puschmann, H. (2009). *J. Appl. Cryst.* **42**, 339–341.

Dridi, R., Dhieb, C., Cherni, S. N., Boudjada, N. C., Sadfi Zouaoui, N. & Zid, M. F. (2018). *J. Mol. Struct.* **1152**, 294–302.

El–Mellouhi, F., Marzouk, A., Bentria, E. T., Rashkeev, S. N., Kais, S. & Alharbi, F. H. (2016). *ChemSusChem* **9**, 2648–2655.

Fuertes, M., Masdeu, C., Martin-Encinas, E., Selas, A., Rubiales, G., Palacios, F. & Alonso, C. (2020). *Molecules* **25**, 3252.

Giese, M., Albrecht, M. & Rissanen, K. (2016). *Chem. Commun.* **52**, 1778–1795.

Groom, C. R., Bruno, I. J., Lightfoot, M. P. & Ward, S. C. (2016). *Acta Cryst.* B**72**, 171–179.

Gural'skiy, I. A., Escudero, D., Frontera, A., Solntsev, P. V., Rusanov, E. B., Chernega, A. N., Krautscheid, H. & Domasevitch, K. V. (2009). *Dalton Trans.* pp. 2856–2864.

Gural'skiy, I. A., Solntsev, P. V., Krautscheid, H. & Domasevitch, K. V. (2006). *Chem. Commun.* pp. 4808–4810.

Hausen, H.-D., Kaim, W., Schulz, A., Moscherosch, M. & Jordanov, J. (1993). *Zeitschrift Für Naturforsch. B* **48**, 1181–1186.

Hirshfeld, F. L. (1977). *Theor. Chim. Acta* **44**, 129–138.

Kobayashi, K., Horiuchi, S., Ishibashi, S., Kagawa, F., Murakami, Y. & Kumai, R. (2014). *Chem. A Eur. J.* **20**, 17515–17522.

Lee, C., Yang, W. & Parr, R. G. (1988). *Phys. Rev. B* **37**, 785–789.

Lee, C.-C., Yuan, C.-H., Liu, S.-W. & Shih, Y.-S. (2011). *J. Display Technol.* **7**, 454–458.

Lee, H., Jeong, K., Cho, S. W. & Yi, Y. (2012). *J. Chem. Phys.* **137**, 034704–034709.

Liao, S.-H., Shiu, J.-R., Liu, S.-W., Yeh, S.-J., Chen, Y.-H., Chen, C.-T., Chow, T. J. & Wu, C.-I. (2009). *J. Am. Chem. Soc.* **131**, 763–777.

Liu, S.-W., Lee, C.-C., Lin, C.-F., Huang, J.-C., Chen, C.-T. & Lee, J.-H. (2010). *J. Mater. Chem.* **20**, 7800–7806.

Magee, T. V., Ripp, S. L., Li, B., Buzon, R. A., Chupak, L., Dougherty, T. J., Finegan, S. M., Girard, D., Hagen, A. E., Falcone, M. J., Farley, K. A., Granskog, K., Hardink, J. R., Huband, M. D., Kamicker, B. J., Kaneko, T., Knickerbocker, M. J., Liras, J. L., Marra, A., Medina, I., Nguyen, T.-T., Noe, M. C., Obach, R. S., O'Donnell, J. P., Penzien, J. B., Reilly, U. D., Schafer, J. R., Shen, Y., Stone, G. G., Strelevitz, T. J., Sun, J., Tait-Kamradt, A., Vaz, A. D. N., Whipple, D. A., Widlicka, D. W., Wishka, D. G., Wolkowski, J. P. & Flanagan, M. E. (2009). *J. Med. Chem.* **52**, 7446–7457.

Mirguet, O., Lamotte, Y., Chung, C., Bamborough, P., Delannée, D., Bouillot, A., Gellibert, F., Krysa, G., Lewis, A., Witherington, J., Huet, P., Dudit, Y., Trottet, L. & Nicodeme, E. (2014). *ChemMedChem* **9**, 580–589.

Nishimura, N., Siegmund, A., Liu, L., Yang, K., Bryan, M. C., Andrews, K. L., Bo, Y., Booker, S. K., Caenepeel, S., Freeman, D., Liao, H., McCarter, J., Mullady, E. L., San Miguel, T., Subramanian, R., Tamayo, N., Wang, L., Whittington, D. A., Zalameda, L., Zhang, N., Hughes, P. E. & Norman, M. H. (2011). *J. Med. Chem.* **54**, 4735–4751.

Park, M. S., Kang, Y.-S., Im, D., Doo, S.-G. & Chang, H. (2014). *Phys. Chem. Chem. Phys.* **16**, 22391–22398.

Perez, C., Li, J., Parlati, F., Rouffet, M., Ma, Y., Mackinnon, A. L., Chou, T.-F., Deshaies, R. J. & Cohen, S. M. (2017). *J. Med. Chem.* **60**, 1343–1361.

Philipsen, P. H. T., te Velde, G., Baerends, E. J., Berger, J. A., de Boeij, P. L., Franchini, M., Groeneveld, J. A., Kadantsev, E. S., Klooster, R., Kootstra, F., Pols, M. C. W. M., Romaniello, P., Raupach, M., Skachkov, D. G., Snijders, J. G., Verzijl, C. J. O., Celis Gil, J. A., Thijssen, J. M., Wiesenekker, G., Peeples, C. A., Schreckenbach, G. & Ziegler, T. (2025). *BAND*. SCM, Theoretical Chemistry, Vrije Universiteit, Amsterdam, The Netherlands. https://www.scm.com.

Plais, R., Clavier, G., Salpin, J., Gaucher, A. & Prim, D. (2023). *Eur. J. Org. Chem.* **26**, e202201281.

Poloek, A., Lin, C.-W., Chen, C.-T. & Chen, C.-T. (2014). *J. Mater. Chem. C* **2**, 10343–10356.

Poloek, A., Wang, C., Chang, Y.-T., Lin, C.-W., Chen, C.-T. & Chen, C.-T. (2015). *J. Mater. Chem. C* **3**, 11163–11177.

Rigaku OD (2024). *CrysAlis PRO*. Rigaku Oxford Diffraction, Yarnton, England.

Schottel, B. L., Chifotides, H. T. & Dunbar, K. R. (2008). *Chem. Soc. Rev.* **37**, 68–83.

Selaković, Ž., Tran, J. P., Kota, K. P., Lazić, M., Retterer, C., Besch, R., Panchal, R. G., Soloveva, V., Sean, V. A., Jay, W. B., Pavić, A., Verbić, T., Vasiljević, B., Kuehl, K., Duplantier, A. J., Bavari, S., Mudhasani, R. & Šolaja, B. A. (2019). *Eur. J. Med. Chem.* **162**, 32–50.

Sheldrick, G. M. (2015*a*). *Acta Cryst.* A**71**, 3–8.

Sheldrick, G. M. (2015*b*). *Acta Cryst.* C**71**, 3–8.

Spackman, P. R., Turner, M. J., McKinnon, J. J., Wolff, S. K., Grimwood, D. J., Jayatilaka, D. & Spackman, M. A. (2021). *J. Appl. Cryst.* **54**, 1006–1011.

Stephens, P. J., Devlin, F. J., Chabalowski, C. F. & Frisch, M. J. (1994). *J. Phys. Chem.* **98**, 11623–11627.

Stevens, J. S., Byard, S. J., Seaton, C. C., Sadiq, G., Davey, R. J. & Schroeder, S. L. M. (2014). *Phys. Chem. Chem. Phys.* **16**, 1150–1160.

Subramanian, S. & Zaworotko, M. J. (1994). *Coord. Chem. Rev.* **137**, 357–401.

te Velde, G. & Baerends, E. J. (1991). *Phys. Rev. B* **44**, 7888–7903.

van den Ham, D. M. W., van Hummel, G. J. & Huiszoon, C. (1978). *Acta Cryst.* B**34**, 3134–3137.

van Lenthe, E., Baerends, E. J. & Snijders, J. G. (1993). *J. Chem. Phys.* **99**, 4597–4610.

van Lenthe, E., Baerends, E. J. & Snijders, J. G. (1994). *J. Chem. Phys.* **101**, 9783–9792.

Wei, H., Zhao, Z., Wei, C., Yu, G., Liu, Z., Zhang, B., Bian, J., Bian, Z. & Huang, C. (2016). *Adv. Funct. Mater.* **26**, 2085–2096.

Wiesner, T., Pardon, M., Maier, S., Rominger, F., Freudenberg, J. & Bunz, U. H. F. (2023). CSD Communication (refcode DIBMOU, CCDC 2155735). CCDC, Cambridge, England.

Zhou, X., Yang, H., Chen, Z., Gong, S., Lu, Z.-H. & Yang, C. (2019). *J. Mater. Chem. C* **7**, 6607–6615.

Zhu, S., Zhang, Q., Gudise, C., Meng, L., Wei, L., Smith, E. & Kong, Y. (2007). *Bioorg. Med. Chem. Lett.* **17**, 6101–6106.

supporting information

Acta Cryst. (2026). E**82**, 1490-1496 [https://doi.org/10.1107/S2056989026012168]

Crystal structure and Hirshfeld surface analysis of 1,5-naphthyridine-1,5-diium dichloride

Valerii Y. Sirenko, Alexandru-Constantin Stoica, Olena V. Prysiazhna, Vadim A. Potaskalov and Irina A. Golenya

Computing details

1,5-Naphthyridine-1,5-diium dichloride

Crystal data

$C_8H_8N_2^{2+}\cdot 2Cl^-$
$M_r = 203.06$
Triclinic, $P\overline{1}$
$a = 4.9408$ (6) Å
$b = 6.3593$ (6) Å
$c = 7.2897$ (8) Å
$\alpha = 81.946$ (8)°
$\beta = 80.375$ (10)°
$\gamma = 80.067$ (9)°
$V = 220.97$ (4) Å^3
$Z = 1$
$F(000) = 104$
$D_x = 1.526$ Mg m^{-3}
Mo $K\alpha$ radiation, $\lambda = 0.71073$ Å
Cell parameters from 1809 reflections
$\theta = 2.8$–30.1°
$\mu = 0.68$ mm^{-1}
$T = 293$ K
Prism, clear colourless
0.19 × 0.05 × 0.04 mm

Data collection

Rigaku XtaLAB Synergy Dualflex diffractometer with a HyPix detector
Radiation source: micro-focus sealed X-ray tube, PhotonJet (Mo) X-ray Source
Mirror monochromator
Detector resolution: 10.0000 pixels mm^{-1}
ω scans
Absorption correction: analytical (CrysAlis PRO; Rigaku OD, 2024)
$T_{min} = 0.911$, $T_{max} = 0.982$
2918 measured reflections
1097 independent reflections
917 reflections with $I > 2\sigma(I)$
$R_{int} = 0.032$
$\theta_{max} = 30.2$°, $\theta_{min} = 2.9$°
$h = -6\rightarrow 6$
$k = -8\rightarrow 8$
$l = -9\rightarrow 9$

Refinement

Refinement on F^2
Least-squares matrix: full
$R[F^2 > 2\sigma(F^2)] = 0.065$
$wR(F^2) = 0.195$
$S = 1.05$
1097 reflections
67 parameters
0 restraints
Hydrogen site location: difference Fourier map
Only H-atom coordinates refined
$w = 1/[\sigma^2(F_o^2) + (0.1455P)^2]$ where $P = (F_o^2 + 2F_c^2)/3$
$(\Delta/\sigma)_{max} < 0.001$
$\Delta\rho_{max} = 0.94$ e Å^{-3}
$\Delta\rho_{min} = -0.40$ e Å^{-3}

Special details

Geometry. All esds (except the esd in the dihedral angle between two l.s. planes) are estimated using the full covariance matrix. The cell esds are taken into account individually in the estimation of esds in distances, angles and torsion angles; correlations between esds in cell parameters are only used when they are defined by crystal symmetry. An approximate (isotropic) treatment of cell esds is used for estimating esds involving l.s. planes.

Fractional atomic coordinates and isotropic or equivalent isotropic displacement parameters (Å²)

	x	*y*	*z*	U_{iso}*/U_{eq}
Cl1	−0.02131 (14)	0.20809 (10)	0.20215 (10)	0.0440 (4)
N1	0.3180 (5)	0.5036 (4)	0.3055 (3)	0.0353 (6)
H1N	0.211 (9)	0.432 (7)	0.284 (6)	0.053*
C1	0.3833 (7)	0.6776 (5)	0.1959 (4)	0.0411 (7)
H1	0.305 (8)	0.705 (6)	0.088 (6)	0.049*
C2	0.5577 (7)	0.8022 (5)	0.2485 (5)	0.0425 (7)
H2	0.604 (8)	0.933 (6)	0.162 (6)	0.051*
C3	0.6580 (6)	0.7484 (4)	0.4140 (4)	0.0361 (6)
H3	0.760 (8)	0.829 (6)	0.448 (6)	0.043*
C4	0.4145 (5)	0.4383 (4)	0.4718 (4)	0.0301 (6)

Atomic displacement parameters (Å²)

	U^{11}	U^{22}	U^{33}	U^{12}	U^{13}	U^{23}
Cl1	0.0466 (6)	0.0465 (5)	0.0482 (6)	−0.0163 (3)	−0.0200 (4)	−0.0099 (3)
N1	0.0339 (13)	0.0406 (12)	0.0373 (13)	−0.0088 (9)	−0.0152 (10)	−0.0082 (10)
C1	0.0424 (17)	0.0471 (16)	0.0375 (15)	−0.0091 (12)	−0.0160 (12)	−0.0020 (12)
C2	0.0476 (18)	0.0393 (15)	0.0433 (16)	−0.0140 (13)	−0.0120 (13)	0.0020 (12)
C3	0.0354 (15)	0.0351 (13)	0.0424 (15)	−0.0115 (11)	−0.0103 (12)	−0.0074 (11)
C4	0.0281 (12)	0.0331 (12)	0.0325 (13)	−0.0073 (9)	−0.0080 (10)	−0.0080 (10)

Geometric parameters (Å, º)

N1—H1N	0.80 (5)	C2—H2	1.01 (4)
N1—C1	1.325 (4)	C2—C3	1.358 (4)
N1—C4	1.362 (3)	C3—H3	0.86 (4)
C1—H1	0.91 (4)	C3—C4^{i}	1.414 (4)
C1—C2	1.396 (5)	C4—C4^{i}	1.391 (5)
C1—N1—H1N	124 (3)	C3—C2—H2	121 (2)
C1—N1—C4	122.5 (2)	C2—C3—H3	120 (3)
C4—N1—H1N	114 (3)	C2—C3—C4^{i}	118.2 (3)
N1—C1—H1	114 (3)	C4^{i}—C3—H3	122 (3)
N1—C1—C2	120.3 (3)	N1—C4—C3^{i}	121.4 (2)
C2—C1—H1	125 (3)	N1—C4—C4^{i}	118.1 (3)
C1—C2—H2	118 (2)	C4^{i}—C4—C3^{i}	120.5 (3)
C3—C2—C1	120.3 (3)		
N1—C1—C2—C3	−1.2 (5)	C1—C2—C3—C4^{i}	1.2 (5)

C1—N1—C4—C3^{i}	−179.9 (3)	C4—N1—C1—C2	0.2 (4)
C1—N1—C4—C4^{i}	0.7 (5)		

Symmetry code: (i) −*x*+1, −*y*+1, −*z*+1.

Hydrogen-bond geometry (Å, º)

D—H···*A*	*D*—H	H···*A*	*D*···*A*	*D*—H···*A*
N1—H1*N*···Cl1	0.80 (5)	2.17 (5)	2.969 (2)	171 (4)
C1—H1···Cl1^{ii}	0.91 (4)	2.67 (4)	3.584 (3)	174 (3)
C2—H2···Cl1^{iii}	1.01 (4)	2.83 (4)	3.532 (3)	127 (3)

Symmetry codes: (ii) −*x*, −*y*+1, −*z*; (iii) *x*+1, *y*+1, *z*.